Condensed matter at ultra-high pressures

B. K. Godwal

An overview of first-principles methods to describe condensed matter over a range of pressures and temperatures where a variety of physical phenomena such as band crossing, phase transitions, ionic and electronic thermal excitations, liquid disorder, pressure and thermal ionization of ionic core, etc., are encountered is presented. The importance of such attempts is shown by comparing their predictions with the results of current high-pressure experiments. Recent developments in first-principles theories and their usefulness in interpreting high-pressure data and in basic and applied sciences are also discussed with emphasis on future scope.

In the recent years pressure has been used as a means of altering the physical and chemical states of materials like varying temperature or chemical composition. The development of the novel diamond anvil cell (DAC) device has revolutionized static high-pressure research. This has enabled measurements of lattice parameters at pressures exceeding 500 GPa[1]. The significance of being able to reach these ultra-high pressures is that the energy density achieved on compression is comparable to bonding energies. Therefore, significant changes are expected, and indeed found, in the electronic states, chemical bonding and atomic packing of condensed matter. In the range of 200–300 GPa pressures, hydrogen is predicted to be metallic[2]. As hydrogen is the most abundant element in the universe, its metallization is not only a dramatic illustration of pressure-induced changes in bonding character, but also plays an important role in determining the internal state and evolution of the giant planets[3,4]. With the advent of laser heating technique it has been possible to heat the samples to several thousand degree celsius in the diamond anvil cell[5,6]. It is expected that static ultra-high pressure and laser heating techniques will be combined in the near future to provide controlled pressure–temperature conditions existing at the centre of the Earth, enabling its major constituents to be studied in the laboratory[7]. Higher pressure–volume-temperature (P–V–T) states are possible with dynamic shock methods, where measurements are carried out along the shock Hugoniot, which represents the locii of all the points reached by shocking the material from a fixed initial state[8]. However, in static compression we have controlled pressure–temperature conditions, while using dynamic methods the temperature remains uncontrolled. Table 1 gives the pressures achieved using various static and dynamic techniques[9]. One of the most important uses of high-pressure experiments is the pressure–volume–temperature relationship of materials, usually defined as the equation of state (EOS). Its measurements and calculations are of immense importance to researchers in both basic and applied sciences. In basic sciences it provides a test to the theoretical models of cohesion and predicts the onset of phase transitions (solid–solid, crystalline–amorphous, solid–liquid, insulator–metal, valence transitions, etc.). EOS is used for pressure calibration in ultra-high pressure experiments above 100 GPa, where the response of the commonly used ruby becomes uncertain[10]. In geophysics it helps to understand the structure of the Earth and in astrophysics to unravel the mysteries of evolution of stellar bodies like white dwarfs, neutron stars and black holes[11]. In applied sciences EOS data serve as vital inputs for hydrodynamical calculations in controlled fission–fusion research, in simulations of reactor accidents and in rock mechanical effects of peaceful nuclear explosions[12–14]. In the recent past considerable theoretical developments have taken place for understanding the response of materials subjected to static and dynamic pressures[15,16]. In brief, when condensed matter is subjected to static and dynamic pressures, various phenomena like phase change, melting, and pressure and thermal ionization effects are encountered till it reaches the extreme high-density thermodynamic state dominated by screened Coulomb interaction.

Thus, the phenomenon encountered at high pressures depends on the range of pressure to which the material is subjected. Pressure density diagram is thus conveniently divided into three regions as shown in Figure 1. Region 1, known as the normal region, extends up to 1000 GPa; for this region extensive shock wave data exist[13] and ultra-high pressure static data using DAC are also becoming available[17]. With the availability of synchrotron radiation and incorporating the excellent features of imaging plate in angle-dispersive X-ray diffraction (ADXRD) set-up[18], highly accurate high-pressure data can be obtained, providing testing ground for various

B. K Godwal is in the High Pressure Physics Division, Bhabha Atomic Research Centre, Trombay, Bombay 400 085, India

Table 1. The highest pressures achieved through various experimental techniques[9–15]

Method	Type of measurement	Maximum pressure (GPa) achieved	Typical V/V_0 achieved	Percentage error in pressure estimation (%)
Static methods				
Piston cylinder	Isotherm	4 5	0 95	3
X-ray diffraction	Isotherm	416	0 4	10
Shock waves	Hugoniot	1000	0 5	2
Chemical explosive	(principal and reflected)			
Gas-gun	Hugoniot (principal and reflected)	500	0 5	1
Laser	Hugoniot (principal and reflected)	3500	0 3	20–30
Underground nuclear explosive	Hugoniot (principal and reflected)	500,000	0 3	2 5
Electric gun	Hugoniot (principal and reflected)	1000–5000	—	—
Rail gun	Hugoniot (principal and reflected)	1000–10,000	—	—
Magnetic compression	Isentrope	500	0 25	—

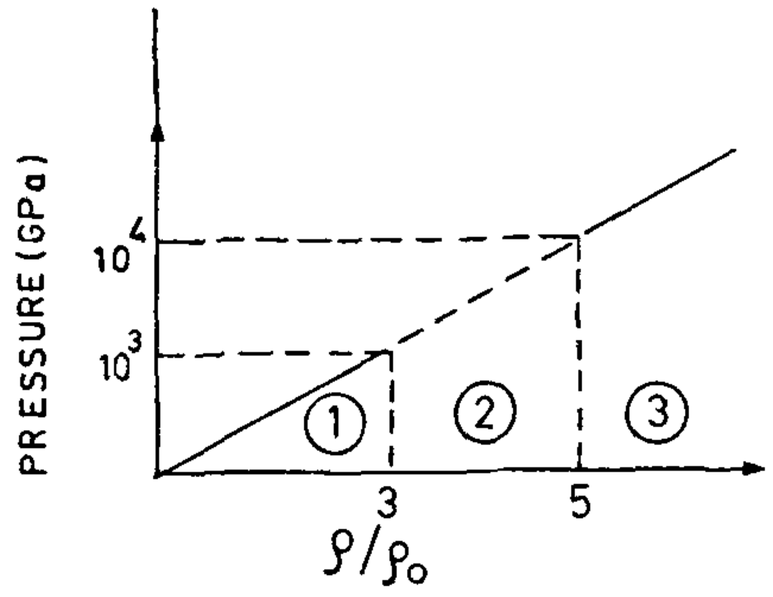

Figure 1. The three regions of the P–V diagram. 1, Normal region $P < 1000$ GPa (experimental), 2, Intermediate region $1000 < P < 10{,}000$ GPa; 3, High density region $P > 30{,}000$ GPa.

condensed-matter theories. The 1000–10,000 GPa pressure range is termed as the intermediate region, for which very few data points are available using underground nuclear explosions and high-power lasers[15]. This region is extremely difficult to approach experimentally because of the requirement of large experimental configurations[19]. Various laboratories in the world are developing new techniques like electric gun, rail gun and magnetic flux compression methods[9,15] to obtain data in this region; however, the reliability and accuracy of such data are yet to be established. Theoretical description of dense heated matter in this region is extremely difficult and in the absence of a complete high-temperature theory, interpolations between the experimental and the high-density regions were made to obtain the thermodynamic data[20]. However, for pressures higher than 30,000 GPa the Fermi nature of electrons forces them into high-momentum states, which results in dominant kinetic energy contribution to the total energy, with potential energy as a small perturbation, enabling various variants of the statistical Thomas–Fermi-Dirac theories[21,22] to be employed for the calculation of the thermodynamic properties.

Theoretical calculations of EOS and predictions of phase transitions thus requires the estimation of free energy F taking into account the underlying physical phenomena in various regions:

$$F = E - TS, \tag{1}$$

where E consists of kinetic and potential energy terms and is obtained from density functional theory, while the contributions to the entropy S at a given temperature T come from thermal excitations of electrons and ions.

Experimental or normal region

For this region we have used a model[23] in which the total energy and pressure at a given volume V and temperature T are divided into three terms:

$$E(V, T) = E_c(V) + E_n(V, T) + E_e(V, T), \tag{2}$$

$$P(V, T) = P_c(V) + \gamma E_T/V + \gamma_e E_e/V, \quad (3)$$

These terms describe the compression of the cold body (i.e. at 0 K), the thermal motion of the ions and the thermal excitations of electrons, γ and γ_e are ionic and electronic Grüneisen parameters. The density-functional-based pseudopotential[23, 24] or the augmented plane wave methods[25] have been used in the past for the evaluation of the cold contribution, while ionic and electronic excitation contributions are obtained, from the phonon frequencies and the electronic band structure, respectively. We have used this formalism for E and P in the Rankine Hugoniot equations to compute the shock Hugoniot of Al[23], for which experimental shock wave data were available and for which there existed discrepancy between the two sets of reported measurements[26, 27]. In Figure 2 we compare our computed Hugoniot pressures with the available experimental data. Our curve is seen to be in good agreement with the data of Al'tshuler *et al.*[26] and Mitchell and Nellis[28], while it differs considerably from the measurements of Skidmore and Morris[27]. Our studies showed that electronic excitation contribution is important, with shock temperatures being extremely sensitive to it. As the temperature rises along the shock Hugoniot at these pressures leads to melting of the solid, we carried out both solid and liquid Hugoniot calculations for Al and other materials[29, 30] (Pb and Au) and found that solid and liquid shock Hugoniots are in mutual agreement with the limits of experimental errors, while the calculated solid and liquid Hugoniot temperatures were very different (Figure 3). Based on these findings we conjectured that melting could be detected by combining theory with shock temperature measurements. Also, in the normal region the excellent agreement observed by us between the calculated and the experimental Hugoniots showed that normal potential continues to remain valid up to these pressures.

Predictions to confirmations

The confirmations of some of the predictions made in the preceding section have come from recent laser-driven shock wave experiments[30]. In order to detect melting in Au, shock temperature measurements were carried out at 600 GPa using laser-driven shock in impedance-mismatched Al–Au target using laser irradiance of 2.3×10^{13} W/cm^2 (0.53 μm, 2–3 ns FWHM). Laser ablation of Al produced a shock wave in Al with a peak pressure of 350 ± 50 GPa at the shock front[31]. Shock reflection at the Al–Au interface then yielded a shock wave of 600 ± 100 GPa in the Au layer. Using Al as the equation of state standard, the shock temperature of Au was determined from the intensity of luminous emission at 4300 Å (in a 100 Å band) from the free surface of the Au layer in the Al–Au target relative to that from the free surface of Al in a shocked, single-layer Al target. Figure 4 shows the experimental set-up used for shock temperature and shock velocity measurements. Figure 5 shows the intensity of luminous emission, as observed using streak camera, from Al and Al–Au targets. The solid and liquid Hugoniots for Au as

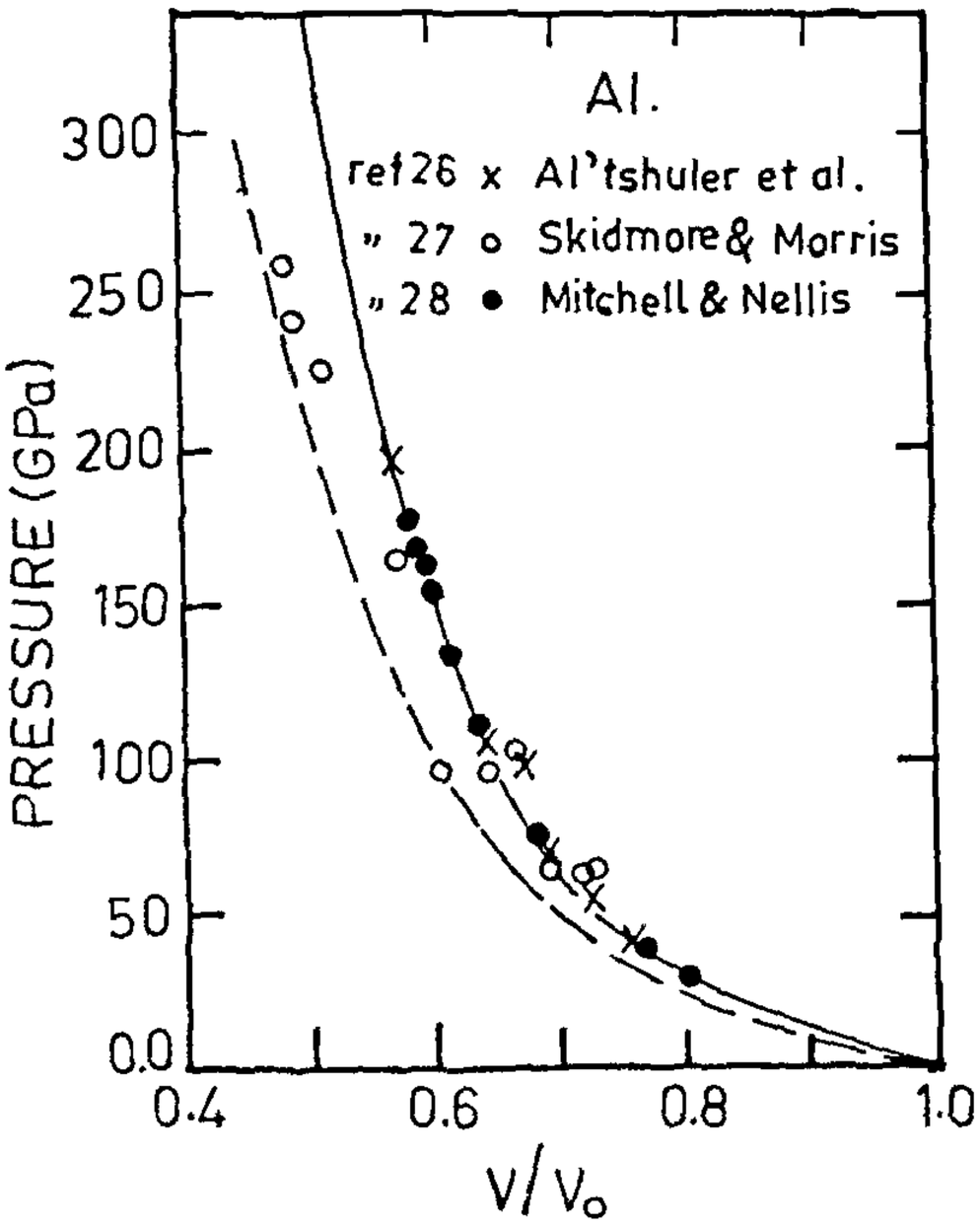

Figure 2. *Comparison of calculated Hugoniot for Al with the available experimental data*[33].

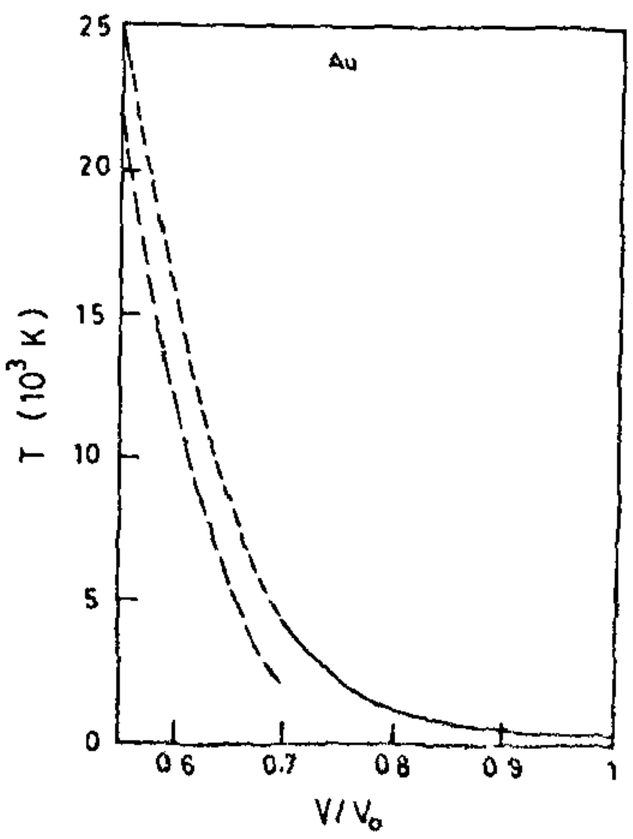

Figure 3. Temperature as a function of compression in Au solid phase calculation (——), liquid phase calculation (– – – –).

calculated using formalisms described by Godwal *et al.*[15] are shown in Figure 6. The measured shock temperature falls on the liquid Hugoniot, indicating that Au was in liquid state[30,31]. Thus, measurements of shock-induced luminescence yielded the first experimental determination of the temperature of Au above the Hugoniot melting point.

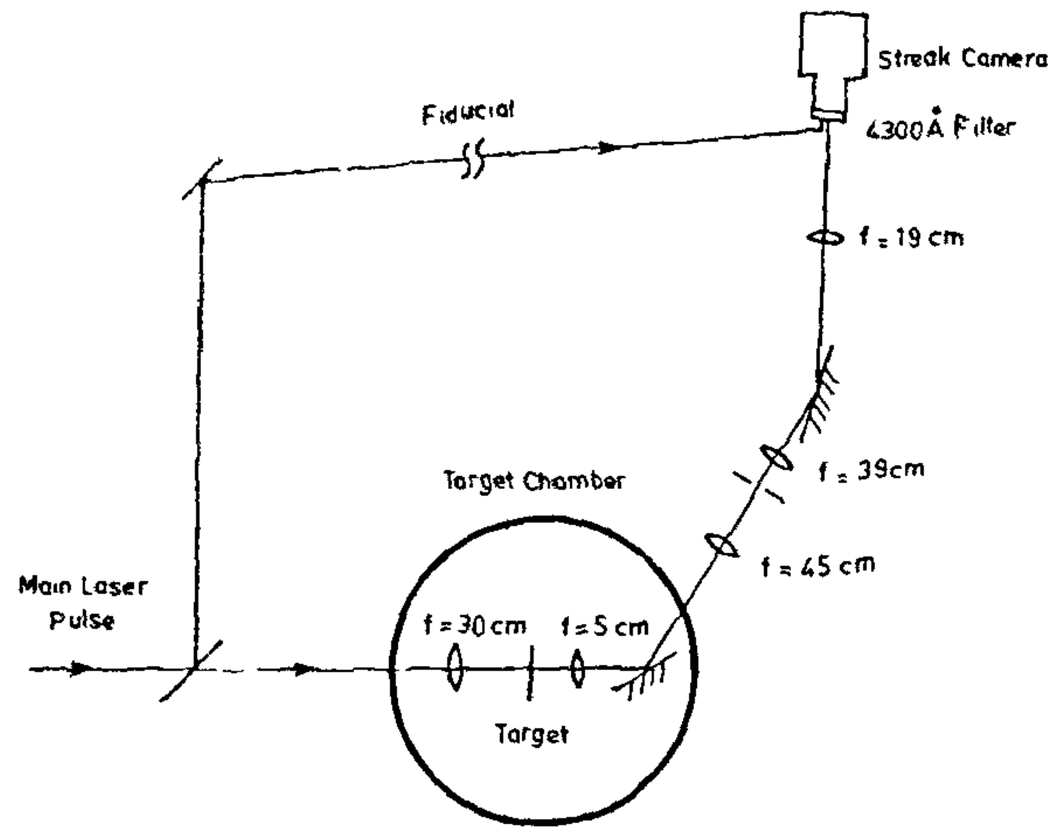

Figure 4. Experimental set up for shock temperature (T_s) and shock velocity (U_s) measurement

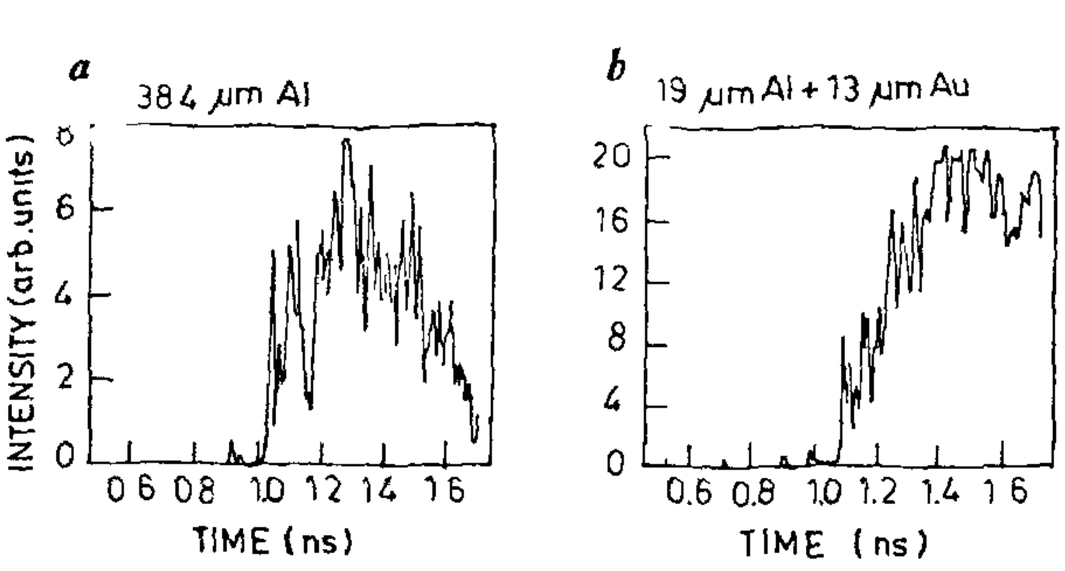

Figure 5. Intensities of luminous emission from a target of (*a*) 38.4 μm Al and (*b*) 19 μm Al + 18.4 μm Au

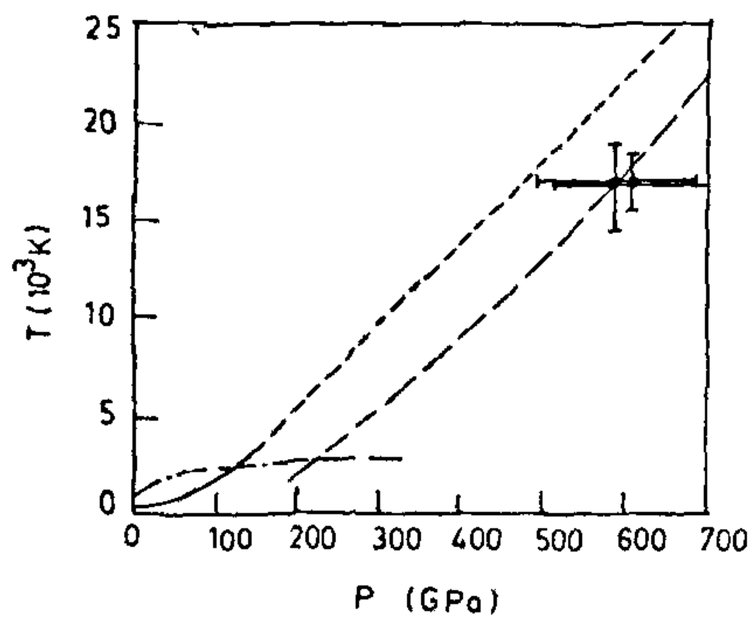

Figure 6. Temperature as a function of shock pressure in Au solid phase calculation (——), liquid phase calculation (– – – –); melting line (– · – · –); SESAME[30] data · · ·; experimental data ●.

With the introduction of linear methods[34] in band theory, the earlier energy band methods are replaced with linear muffin tin orbital (LMTO) and linearized augmented plane wave (LAPW) methods[34,35]. These methods are about order of magnitude times faster and are ideally suited for the calculations of total energies of the solid, which require about 1000 $\vec{k}$ points sampling for elemental solids. Thus, starting with only atomic numbers of the constituent elements, the total-energy calculations of electrons in the static periodic arrays of ions can predict the structural stabilities of solids without the need to adjust any parameter empirically. These powerful theoretical means are proving to be extremely useful in finding new materials and for predicting their behaviour under static and dynamic pressures[15,36,37]. The predicted structural sequences and their transition pressures are in excellent agreement with the experimental observations and have been discussed elsewhere[38,39]. It is noteworthy to mention that the electronic structure of high-Z element Th, for which relativistic effects become important, was studied by us recently[36]. We found that elemental thorium is unique in that unoccupied f level becomes populated at ultra-high pressures, with the Fermi level intercepting the f band at a volume fraction of 0.6. The total energies show that the resulting occupation of f bands by about one electron drives the fcc to body centred tetragonal (bct) transition near 80 GPa pressure, and Th then resembles the f band metal Ce. It is to be noted that such details about the microscopic mechanism driving the phase transition are possible as a result of *ab initio* studies.

The other laser-driven shock experiment involved the measurement of K-photoabsorption edge of shocked aluminium[32]. The high-power Nd–YAG laser with 0.53 μm, 2–3 ns FWHM at irradiance of $2\text{–}3 \times 10^{13}$ W/cm^2 was used to produce a 350 GPa shock in Al. The X-rays produced in the laser-produced plasma side were used to back-light the target. The time-resolved spectroscopic measurements were used to measure the time evolution of the K-photoabsorption edge. The measurements showed a maximum red shift of about 10 eV, consistent with the theoretical calculation of the Al K-edge with no change of Al normal potential up to these shock pressures[33], confirming again our predictions of the constancy of potential in the normal region.

Current energy band methods

Elemental solids to large systems

The electronic structure calculations based on solutions of Kohn–Sham equations[40] are extremely time-consum-

ing, especially when the periodic unit cell possesses many atoms. In the absence of supercomputers it is impossible to obtain the solution of the electronic structure for determining the physical properties for such large systems. However, with the development of recent parallel processing technique it is now possible to perform complicated calculations of electronic structure for systems with several hundreds of atoms in the unit cell. We used the recently developed parallel processing system at BARC referred as BPPS[41], to perform electronic structure calculations on ©-$Mg_{32}Zn_{48}$ system[42], where © denotes the central site of the packing unit, with Zn, Mg, Al and vacancy at ©. We employed parallelized muffin-tin orbital program and the calculations in the body-centred cubic (bcc) structure are related to the 1/1 crystal approximant to the Al–Zn–Mg quasicrystal. The results of 0 K ground state total-energy calculations are shown in Table 2, which shows that the occupation of the central site of Al or Zn atom is preferred to the vacant centre. It is also observed that Mg atom is not a probable occupant of the central site due to its large size. These calculations fully support the positron annihilation experiments which reveal that centres of packing units are occupied. Figure 7 shows the electronic density of states and the Fermi level E_F for the crystal approximant with Al- centred case. The density of states curves show only shallow minimum (valley) near E_F (indicating a small so-called pseudogap) which is consistent with the fact that experimental specific heat data for the Al–Zn–Mg quasicrystal is almost free-electron-like. Having shown the feasibility of electronic structure calculations for a large system with 162 atoms per unit cell-like crystal approximant ($Zn_{48}Mg_{32}$) to Al–Zn–Mg quasicrystal, we are now carrying out electronic structure calculations for novel materials like superlattices, superconductors and C_{60} at ambient and high pressures[43–45].

We also applied the first-principles linear muffin-tin orbital theory to interpret the high-pressure experimental data obtained by us for the intermetallic compound $AuIn_2$. It crystallizes in CaF_2 structure and is important in geophysical studies because many of the oxides have this phase. Storm *et al.*[46] have made studies for its fusion curve under pressure and observed a change of slope around 3 GPa suggesting phase transition. In order to confirm this we investigated $AuIn_2$ using electrical resistivity, thermoelectric power and high-pressure angle-dispersive X-ray diffraction[47]. The results of these studies are shown in Figure 8, which shows that the resistivity curve changes slope around 3 GPa while our ADXRD measurements reveal structural phase transition around 15 GPa from its ambient CaF_2 structure[46]. The results of thermoelectric power measurements carried out on this compound (Figure 9) show rapid increase in thermoelectric power around 2 GPa. As these measurements are sensitive to electronic rearrangements, the 3 GPa transition observed by Storm *et al.*[46] and confirmed by our resistivity and thermoelectric power measurements seems to be isostructural and associated with electronic structure changes. In order to corroborate it by first-principles theory, we carried out detailed band structure studies by LMTO method in the CaF_2 phase up to a pressure of 10 GPa. In our calculations we included the relativistic spin-orbit correction terms. The density of states at the Fermi level (E_F) obtained from the details of band structure calculations show a 2–3% change up to a pressure of 4 GPa, consistent with our experimental

Table 2. Total energy comparison with and without atom at the centre of packing unit (muffin-tin correction included)

Atom at central site	Total energy (valence) of atom (Ryd)	Total energy per primitive cell (Ryd)	Total energy of empty centred crystal + a well-separated atom (Ryd)
Empty sphere	—	−169 122	−169 122
Al	−4 050	−173 280	−173 172
Mg	−1.763	−170 861	−170 885
Zn	−2.247	−171 434	−171 369

Aluminium centres are most stable.
Zinc at centres is more stable than at empty centres
Magnesium at the centres is not stable (atoms are large)

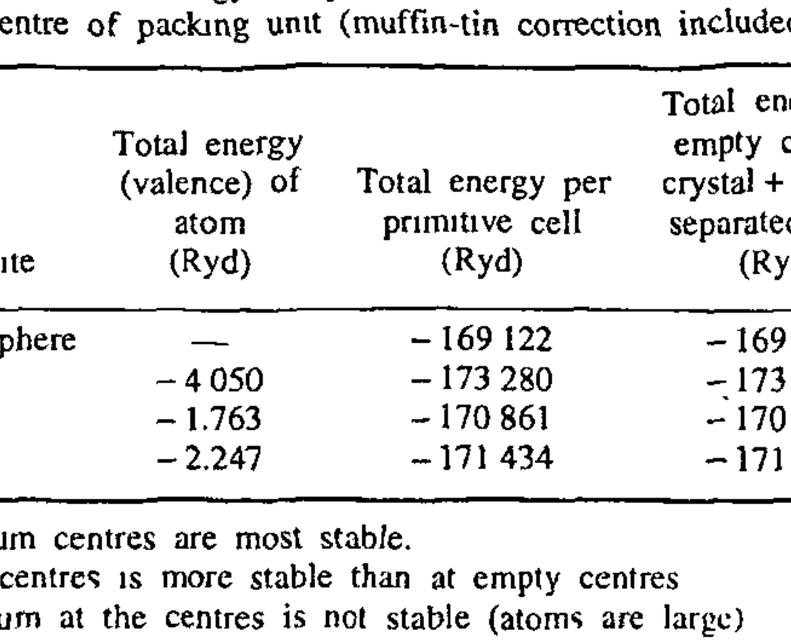

Figure 7. Density of states for Al-$Mg_{32}Zn_{48}$ showing a shallow pseudogap at Fermi level

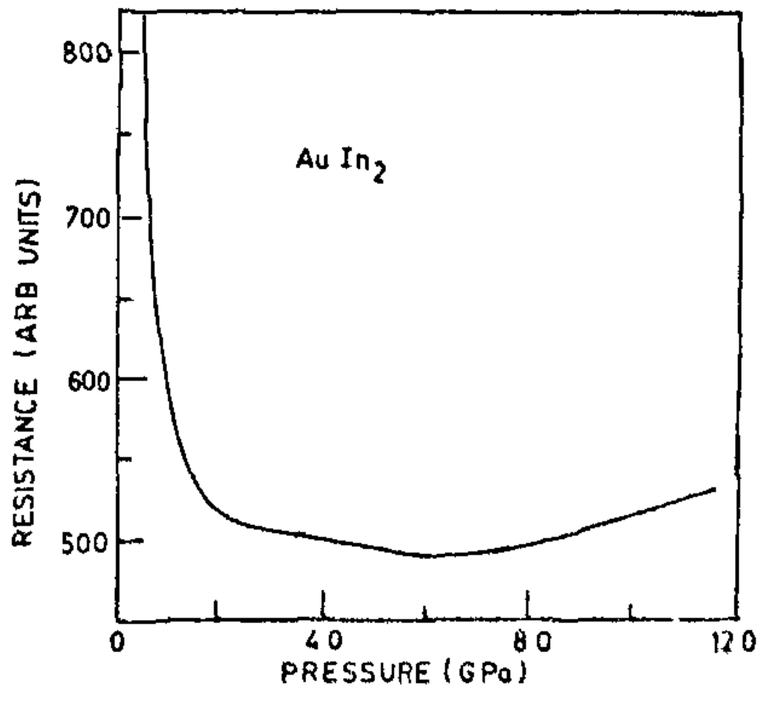

Figure 8. Variation of resistance with pressure for $AuIn_2$

observation of resistivity variation with pressure. We find from Figure 10 that the X_3–Γ_2–L_1 band, which is occupied at normal pressure, shifts upward with respect to Fermi energy and becomes almost flat in the Γ–X direction near the Γ-point in the 2–4 GPa pressure range. This gives additional hole sheet contribution to the Fermi surface as the Γ_2 level moves up through E_F. These features of electronic band structure result in Lifshitz singularity[48] in the density of states and are related to the high-pressure fusion behaviour, electric resistivity variation and thermo electric power measurements.

Intermediate region

In the intermediate region the experimental data are sparse and pressure and thermal ionization effects controlled by atomic shell structure effects dominate many physical properties[15]. Attempts have been made to approach this region from the high-density side with inclusion of shell effects in Thomas–Fermi–Dirac theory[49 50]. Essentially, in this approach one starts with Thomas–Fermi potential and treats the atom more quantum-mechanically. At a given density and temperature one estimates the number of bound electrons and then fixes the chemical potential from the actual free electrons. The details of this approach for the evaluation of thermodynamic properties and the self-consistent field model of Liberman[51], which tries to approximate the potential in a muffin-tin way, are discussed in detail by Godwal *et al.*[15]. However, all these methods lack the solid-state band effects and are not suitable for use in the intermediate region.

We approached the intermediate region[52] from the normal experimental region side by including the pressure and thermal ionization effects using the Saha ionization theory, modified for high-density effects like lowering of ionization potential, partition function cut-off and pressure ionization[53]. The pressure and thermal ionization effects cause core ionization and bring about core conduction electron coupling, thus violating the orthogonality condition which keeps the conduction and core electrons decoupled. Thus, the normal valence charge Z changes to Z_{PT} at a given density and temperature and alters the potential parameters. This particular pressure and thermal ionization state with ionization excitation contribution is then treated using the solid or liquid state models with ionic and electronic excitation included in the total energy (see Figure 11). The pressure and thermal ionization effects estimated using this approach are given in Table 3, which show that Al and Mo indeed show pressure and thermal ionization effects at these pressures. The justification for the use of modified Saha ionization theory in the presence of strong interactions was provided by estimating the valence charges of solids at ambient condition and by simulating the experimentally observed valence transition in Eu[54]. The shock Hugoniot for Al computed using this theory is shown in Figure 12. It can be seen that in the experimental region, it agrees well with the data of Al'tshuler *et al.*[55]. We also compared our Hugoniot with the data of Al'tshuler *et al.*[56] in the intermediate region but here there is poor agreement. However, it may be added that the interpolation shock adiabat obtained by Al'tshuler *et al.*[56] based on their experimental data and the Thomas–Fermi model heavily overpredict the compression at 1.085 TPa compared to the experimental measurement of Volkov *et al.*[57]. On the other hand, there is excellent agreement of this experimental point with our theoretical model as shown in Figure 12.

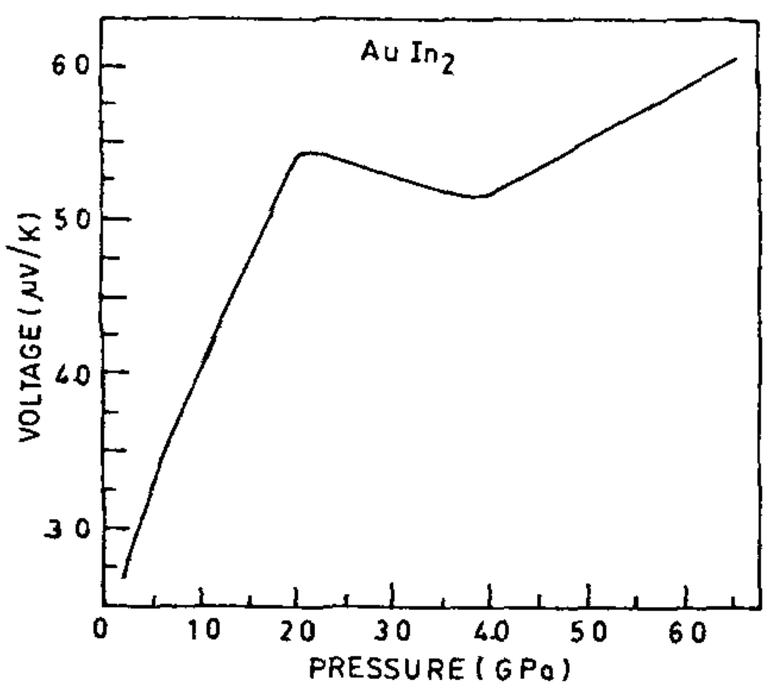

Figure 9. Variation of thermoelectric power with pressure for $AuIn_2$

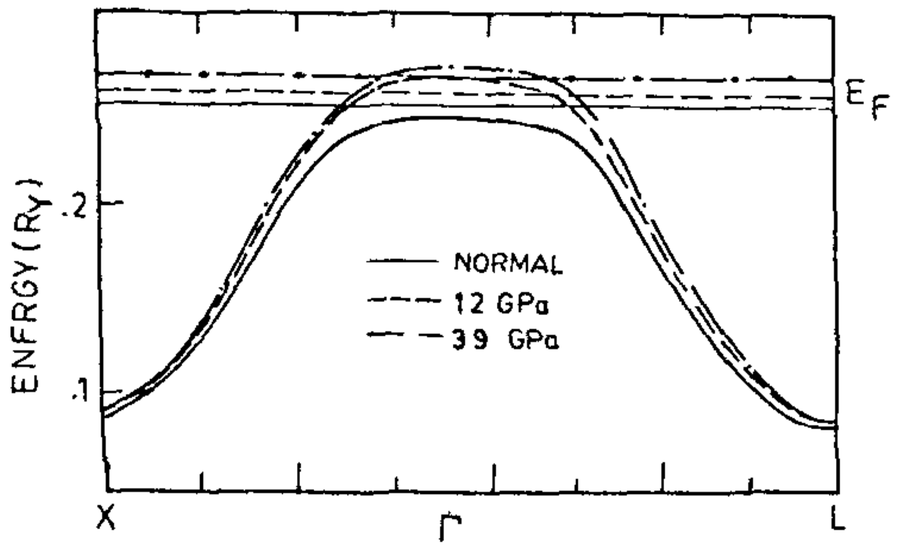

Figure 10. Band crossing across Fermi level with pressure in $AuIn_2$

First-principles simulations

We are currently working on the first-principles simulation method commonly known as the Car–Parrinello method[58] to obtain the changes in the potential parameters and the unknown structure as a result of phase change; this avoids an intelligent guess to be made while making this search using first-principles total-energy calculations.

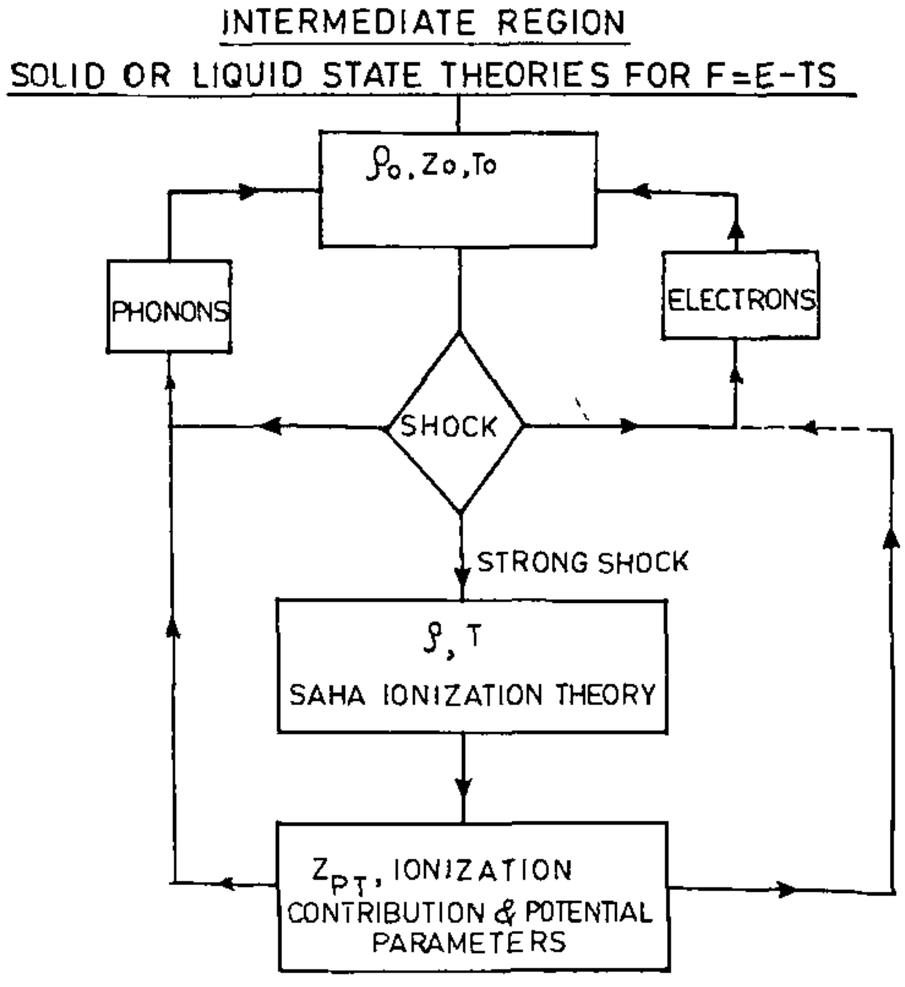

Figure 11. Schematic diagram illustrating the equation of state model in the intermediate region.

Table 3. Pressure and thermal ionization effects along the Hugoniot

Element	V/V_0	Z_P	Z_{PT}
Mo	0 331	6 1	8 1
	0 250	6 8	
	0.150	8.0	
	0 100	8 4	
	0 050	12 0	
Al	0 350	3.0	3.0
	0 300	3 0	3.2

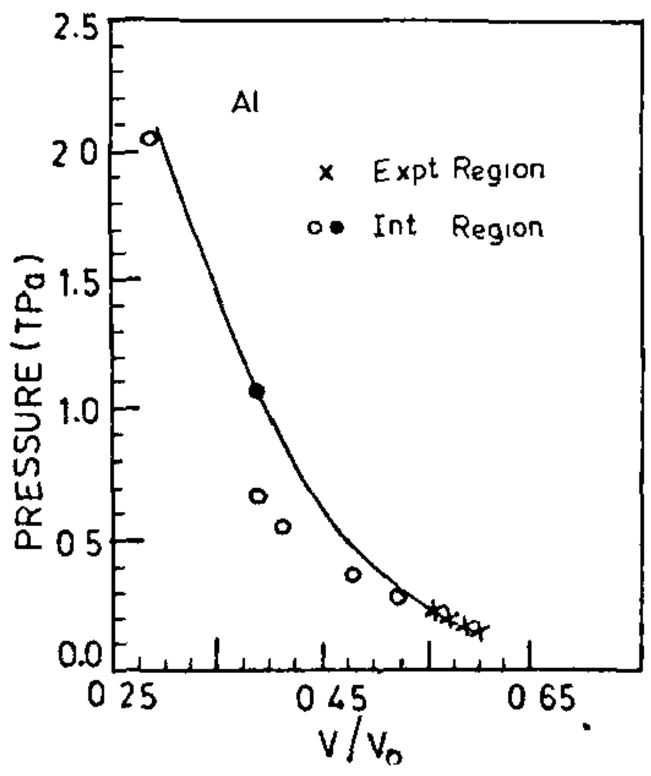

Figure 12. Comparison of computed shock Hugoniot for Al with experimental data in the intermediate and experimental regions[52]. The crosses are from ref 55 while open circles are from ref. 56 and the dot refers to Volkov *et al.*'s point[51].

These simulations are also extremely important to study the atomistic shock propagation in materials[59], to interpret the current shock experiments[60, 61] and for modelling the material behaviour under strong shocks which might lead to pressure and thermal ionization effects. In these simulations the quantum-mechanical many-body problem is mapped into the classical space with treatment of the electron wave functions and the ionic coordinates as the generalized coordinates and the potential energy appearing in the fictitious Lagrangian to be obtained from the density functional theory. The fast Fourier transforms (FFT) are called many times in the Car–Parinello method. We have used BPPS to parallelize the FFT part, achieving a speed-up of 6 for FFT as compared to sequential version[62]. This method is currently being applied to study the structure of the amorphous phase of sulphur[63]. Sulphur is known to amorphize at about 25 GPa at ambient temperature. Regarding the mechanism of this amorphization, there are two possibilities: (i) kinetic hindrance of S_8 molecules for transformation to another crystalline phase of higher symmetry and (ii) breaking of S–S bond within an S_8 molecule. We have carried out simulated annealing on a model system of 27 S atoms with density corresponding to 25 GPa pressure. The purpose of the simulation is to see if the S_8 rings exist in general in many phases of S. Our initial results using coupled density functional molecular dynamics simulations do not show up the S_8 rings.

The propagation of shock waves in condensed matter and the establishment of thermodynamic equilibrium behind it are still not understood and first-principles simulations are ideally suited to study this and interpret the current shock experiments carried out to understand the microscopic mechanism of shock propagation in condensed matter[9].

Conclusions

We observe that theory provides a powerful means for the predictions and interpretation of high-pressure data. With the advent of supercomputing techniques it is now possible to study complex systems for their normal and high-pressure behaviour, which has important applications in design and synthesis of new materials. Also, theoretical studies have been made to show that diamond is stable against structural phase transition and metallization for pressures above 1000 GPa. It is thus expected that high yield strength diamonds will be able to generate pressures higher than 500 GPa. The coupling of laser heating technique with ultra-high pressures shall provide pressure–temperature conditions which otherwise were possible only using dynamic shock methods. The interpretation of such static and shock data by first-principles theories shall help in the development of proper high-

temperature theory and better microscopic understanding of shock temperature. As the pressure region reaches 1000 GPa, we expect to observe pressure ionization and its effect on material properties. Study of materials with various techniques at low pressures continues to remain an active area of research and interpretation of such experiments using first-principles theories continues to pay rich dividends. However, the basic limitation of band structure methods is their inability to predict structure with lowest free energy although they can be used to determine the most stable structure from a variety of trial structures. The first-principles coupled density functional molecular dynamical simulations can be used to discover the structure of lowest-energy state and is perhaps the only technique to be applied under extreme conditions of pressure and temperature when the simulations based on empirical potential are no longer valid, for example, due to core ionization and the resulting core conduction electron coupling. With the efforts aimed at further parallelization of coupled density functional molecular dynamics code, it will be possible to make simulations at arbitrary temperature and matter density for phenomena under equilibrium and nonequilibrium conditions.

The high-power lasers are proving to be an important tool to observe new phenomena. In spite of the fact that there are large error bars on measured shock temperatures, these have been unambiguously associated with shock melting of solid. Photo absorption edge spectroscopy provides important information regarding pressure and thermal ionization under shock compression and shall be an active area of research in the near future. Also the first-principles simulations shall provide deeper understanding of the ultra-fast phenomena under laser–material interaction.

The multidisciplinary nature of high-pressure research with wide applications in various areas of basic and applied sciences is undoubtedly clear. With the introduction of newer techniques the high-pressure data will provide a testing ground for the development of new theories. Such intense interaction between theory and experiments will be of significant importance to other areas of basic sciences and for the generation of high-pressure data for materials for a variety of applications.

1. Ruoff, A. L., in *Recent Trends in High Pressure Research* (ed. Singh, A. K) Oxford & IBH, New Delhi, 1991, p. 769; Ruoff, A. L., Xia, H, Luo, H. and Vohra, Y. K., *Rev. Sci Instrum.*, 1990, **61**, 3830; Vaidya, S N. and Kennedy, G. C., *J. Phys. Chem. Solids*, 1970, **31**, 2329.
2. Mao, H K. and Hemley, R. J., *Rev Mod. Phys.*, 1994, **66**, 671.
3. Stevensen, D J, *Annu. Rev. Earth Planet Sci*, 1982, **10**, 257.
4. Hubbard, W. B, *Planetary Interiors*, Van Nostrand Reinhold, New York, 1984, p 334.
5. Heinz, D. L. and Jeanloz, R., *J. Appl. Phys.*, 1984, **55**, 885
6. Godwal, B. K., Meade, C., Jeanloz, R., Garcia, A., Liu, A. Y. and Cohen, M L., *Science*, 1990, **248**, 462
7. Stacey, F. D, *Physics of the Earth*, Wiley, New York, 1969.
8. Zel'dovich, Yu. B. and Raizer, V. P., *Physics of Shock Waves and High-Temperature Hydrodynamics Phenomena*, Academic, New York, 1967.
9. Chidambaram, R. and Sharma, S. M, *Curr Sci*, 1991, **60**, 397.
10. Mao, H. K. and Hemley, R. J., *Nature*, 1991, **351**, 721.
11. Schwarzschild, M, *Structure and Evolution of the Stars*, Princeton University Press, 1958
12. Chidambaram, R. and Ramanna, R., in *Proc. Tech. Commun. PNE 4*, International Atomic Energy Agency, Vienna, 1995, p 421.
13. Godwal, B K. in *IPA Seminar on Physics on Fusion Plasmas*, Matheran, Dec. 1982, pp. 1–22.
14. Chidambaram, R, Sikka, S. K. and Gupta, S C., *Pramana – J. Phys.*, 1985, **24**, 245.
15. Godwal, B K., Sikka, S. K. and Chidambaram, R., *Phys. Rep.*, 1983, **102**, 121.
16. Ross, M., *Rep. Prog Phys*, 1985, **48**, 1.
17. Vohra, Y. K. and Akella, J., *Phys. Rev Lett.*, 1991, **67**, 3563.
18. Takemura, K., *Phys. Rev.*, 1991, **B44**, 545.
19. Ragan III, C. E., *Phys. Rev.*, 1982, **A25**, 3360.
20. Ragan III, C. E., Silbert, M G. and Diven, B. C., *J. Appl. Phys*, 1977, **48**, 2860.
21. McCarthy, S. L., Lawrence Livermore Laboratory Report UCRL, 1965, p 14364
22. More, R. M., *Phys. Rev.*, 1979, **A19**, 1234.
23. Godwal, B K., Sikka, S. K. and Chidambaram, R., *Phys. Rev.*, 1979, **B20**, 2362.
24. Friedli, C. and Ashcroft, N. W., *Phys. Rev. B.*, 1975, **12**, 5552.
25. Ross, M. and McMahan, A. K., *Phys. Rev. B.*, 1977, **15**, 718.
26. Al'tshuler, L. V., Kormer, S. B., Braznik, M. I., Vladimirov, L. A., Speranskya, M P.. and Funikov, A I, *Sov. Phys. JETP*, 1960, **11**, 766, Al'tshuler, L. V., *Sov. Phys. Uspekhi*, 1965, **8**, 52; Al'tshuler, L. V., Kormer, S. B., Bakanova, A. A. and Trunin, F., *Sov. Phys. JETP*, 1960, **11**, 573.
27. Skidmore, I. C. and Morris, E., in *Thermodynamics of Nuclear Materials*, IAEA, Vienna, 1962, p 173.
28. Mitchell, A. C. and Nellis, W. J., *J. Appl. Phys.*, 1981, **52**, 3363.
29. Godwal, B. K., Sikka, S. K. and Chidambaram, R., *Pramana – J Phys.*, 1987, **29**, 93.
30. Godwal, B. K., Ng, A. and DaSilva, L., *Phys. Lett.*, 1990, **144**, 26.
31. Ng, A., Chiu, G., DaSilva, L., Godwal, B. K. and Cottet, F., *Opt. Commun.*, 1989, **72**, 297.
32. DaSilva, L., Ng, A., Godwal, B. K., Chiu, G. and Cottet, F., *Phys. Rev. Lett.*, 1989, **62**, 1623.
33. Godwal, B. K., Ng, A., DaSilva, L., Lee, Y. T. and Liberman, D. A., *Phys. Rev.*, 1989, **A40**, 4521.
34. Andersen, O. K., *Phys. Rev.*, 1975, **B12**, 3060; Skriver, H L., *The LMTO Method*, Springer, Berlin, 1984.
35. Singh, D. and Papa Constantopolous, *Phys. Rev.*, 1990, **B42**, 8885.
36. Rao, R S., Godwal, B. K. and Sikka, S. K., *Phys. Rev*, 1992, **B46**, 5780.
37. Gupta, S. C., Daswani, J. M., Sikka, S. K. and Chidambaram, R., *Curr. Sci.*, 1993, **65**, 399.
38. Meenakshi, S, Godwal, B K., Rao, R. S. and Vijayakumar, V., *Phys. Rev.*, 1994, **B50**, 6569.
39. Meenakshi, S., Vijayakumar, V., Godwal, B. K and Sikka, S K, *Phys. Rev*, 1993, **B46**, 14359.
40. Kohn, W. and Sham, L. J., *Phys. Rev.*, 1965, **A140**, 1133
41. Dhekne, P. S., Ramesh, K., Rajesh, K., Mahajan, S. M. and Kaura, H K., *Electronics Today*, 1993, **26**, 76.
42. Rao, R. S, Godwal, B. K., Sikka, S. K. and Chidambaram, R., *Phys. Rev.*, 1994, **B50**, 15632.
43. Rao, R. S., Godwal, B. K., Sikka, S. K. and Chidambaram, R, to be communicated to *Curr. Sci.*, 1995.

44. Meenakshi, S., Vijayakumar, V., Godwal, B. K, Sikka, S K., Hossuin, Z, Nagarajan, R., Gupta, L. C. and Vijayaraghavan, R., *Solid State Phys. (India)*, 1994, **C37**, 352
45. Rao, R S., *Solid State Phys. (India)*, 1994, **C37**, 15
46. Storm, A. R., Wernick, J. H. and Jayaraman, A, *J. Phys. Chem. Solids*, 1966, **27**, 1227.
47. Godwal, B. K., Jayaraman, A., Meenakshi, S, Rao, R. S., Sikka, S. K. and Vijayakumar, V., *Solid State Phys. (India)*, 1994, **C37**, 423.
48. Ziman, J. M., in *Principles of the Theory of Solids*, Cambridge University Press, Cambridge, 1964.
49. Zink, J. W., *Phys. Rev.*, 1968, **176**, 279.
50. Rozsnyai, B. F., *Phys. Rev.*, 1972, **A5**, 1137.
51. Liberman, D., *Phys. Rev.*, 1979, **B20**, 4891
52. Godwal, B. K., Sikka, S. K. and Chidambaram, R., *Phys. Rev. Lett.*, 1981, **47**, 1144.
53. Rouse, C. A., in *Progress in High-Temperature Physics and Chemistry*, vol. 4 (ed. Rouse, C. A), Pergamon Press, New York, 1971, p. 139.
54. Godwal, B. K., *Phys. Rev.*, 1983, **A28**, 1103.
55. Al'tshuler, L. V., Kormer, S. B., Braznik, M. I., Vladimirov, L. A., Speranskaya, M. P. and Funtikov, A. I., *Sov. Phys. JETP*, 1960, **11**, 766.
56. Al'tshuler, L. V., Kalitkin, N. N., Kuz'min and Chekin, B. S., *Sov. Phys. JETP*, 1977, **45**, 167.
57. Volkov, A. P., Voloshin, N. P., Vladimira, A. S., Nogin, V. N. and Simonenko, V. A., *Sov. Phys. JETP Lett.*, 1980, **31**, 588.
58. Car, R. and Parrinello, M., *Phys. Rev. Lett.*, 1985, **55**, 2471.
59. Chidambaram, R., *Bull. Mater. Sci.*, 1984, **6**, 633.
60. Johnson, Q. and Mitchell, A., *Phys. Rev. Lett.*, 1972, **29**, 1369.
61. Whitlock, R. R., Wark, J. S. and Kiehm, G., *Shock Compression of Condensed Matter*, (ed. Schmidt, S. C., Johnson, J. N. and Davison, I. W.), Elsevier, Amsterdam, 1990, pp. 897 and 901.
62. Jagadeesh, B. S., Rao, R. S. and Godwal, B. K., in *Super Computing for Scientific Visualization* (ed. Mahajan, S., Mani, H. K., Guruvayurappan and Dhekne, P. S.), p. 165.
63. Luo, H. and Ruoff, A. L., *Phys. Rev.*, 1993, **B48**, 56.

ACKNOWLEDGEMENTS. I acknowledge my association with Drs R. Chidambaram and S. K. Sikka during the course of this work and am extremely grateful to them for their help and several helpful suggestions.

Errata

Morphology and glacier dynamics studies in monsoon–arid transition zone: An example from Chhota Shigri Glacier, Himachal-Himalaya, India

D. P. Dobhal, Surendar Kumar and A. K. Mundepi

(*Current Science*, 1995, **68**, 936–944)

1. Page 936, para 1, line 14, read the per day discharge . . . 85 and 2000 tons in 1988–1989.
2. Page 936, para 5, line 1, read 32°11′–32°17′ N in place of 32°11′–32°17″ N.
3. Page 936, Table 1, line 20, add (average 7.5 m y^{-1}) in line 19.
4. Page 936, Table 1, line 22 read ice volume in water equivalent 572,921.1 × 10^9 m^3 in place of 572,910^9 m^3.
5. Page 943, para 2, line 14 (w. eq. = 572,921.1 × 10^9 m^3) in place of (w. eq. = 572,921 × 10^9 m^3).
6. Page 943, para 3, (mass balance), line 15 and 16 read -1.01×10^6 m^3 and -1.7×10^6 m^3 in place of 1.01×10^6 m^3 and 1.7×10^6 m^3.
7. Page 944, reference 5, read 44 in place of 144.

Stereochemistry of Organic Compounds – Principles and Applications. D. Nasipuri. Wiley Eastern, New Delhi.

The review of the above book by R. Balaji Rao published in the 25 April issue of *Current Science* (1995, **68**, 850) was erroneously reprinted in the 25 May issue of *Current Science* (1995, **68**, 1064). The error is regretted.

— *Editors*